JBC RESEARCH ARTICLE

Genome-wide CRISPR activation screen identifies JADE3 as an antiviral activator of NF-kB–dependent IFITM3 expression

Received for publication, September 29, 2023, and in revised form, February 29, 2024 Published, Papers in Press, March 9, 2024,
https://doi.org/10.1016/j.jbc.2024.107153

Moiz Munir[1], Aaron Embry[1], John G. Doench[2], Nicholas S. Heaton[3], Craig B. Wilen[4], and Robert C. Orchard[1,*]

From the [1]Departments of Immunology and Microbiology, University of Texas Southwestern Medical Center, Dallas, Texas, USA; [2]Broad Institute of MIT and Harvard, Cambridge, Massachusetts, USA; [3]Department of Molecular Genetics and Microbiology, Duke University School of Medicine, Durham, North Carolina, USA; [4]Department of Laboratory Medicine and Immunobiology, Yale School of Medicine, New Haven, Connecticut, USA

Reviewed by members of the JBC Editorial Board. Edited by Craig Cameron

The innate immune system features a web of interacting pathways that require exquisite regulation. To identify novel nodes in this immune landscape, we conducted a gain-of-function, genome-wide CRISPR activation screen with influenza A virus. We identified both appreciated and novel antiviral genes, including Jade family PHD zinc finger 3 (JADE3) a protein involved in directing the histone acetyltransferase histone acetyltransferase binding to ORC1 complex to modify chromatin and regulate transcription. JADE3 is both necessary and sufficient to restrict influenza A virus infection. Our results suggest a distinct function for JADE3 as expression of the closely related paralogs JADE1 and JADE2 does not confer resistance to influenza A virus infection. JADE3 is required for both constitutive and inducible expression of the well-characterized antiviral gene interferon-induced transmembrane protein 3 (IFITM3). Furthermore, we find JADE3 activates the NF-kB signaling pathway, which is required for the promotion of IFITM3 expression by JADE3. Therefore, we propose JADE3 activates an antiviral genetic program involving NF-kB–dependent IFITM3 expression to restrict influenza A virus infection.

The innate immune system consists of dynamic signaling networks that have substantial overlap and feedback loops to precisely tune the timing, magnitude, and duration of inflammation (1). Inflammation is a classic biological example of a double-edge sword since inflammation is critical for clearing pathogenic invaders, but uncontrolled inflammation can lead to tissue damage and is a hallmark of autoimmunity. Despite over 50 years of research, our understanding of essential regulators of innate immunity remains incomplete due to the interwoven and convoluted nature of the signaling cascades.

CRISPR/Cas9 genetic engineering has enabled scientists to perturb mammalian genomes with unprecedented precision and scale (2, 3). Genetic screens using CRISPR/Cas9 and related technologies have increased our understanding of innate immune signaling through the systematic identification of positive and negative regulators of cytokine signaling (4–8). While most screens have focused on loss-of-function phenotypes, modifications to the CRISPR/Cas9 system enable gain-of-function screening through the transactivation of gene expression (9). This CRISPR activation (CRISPRa) approach enables the identification of key bottlenecks in biological systems and overcomes genetic redundancy, which may provide novel insight into the wiring of innate immune circuits.

Pathogens are excellent tools to study innate immunity since pathogens and immune systems coevolved together. Pathogens are not only sensed by the innate immune system but also employ counter measures to circumvent cellular restriction factors. Thus, leveraging the selective pressure of pathogens such as viruses is a powerful screening approach to identify important genes involved with the immune system. Influenza A virus (IAV) is a segmented, negative sense RNA virus that is a significant cause of human disease annually with pandemic potential. While innate immune responses to IAV are critical for establishing control of viral replication, our understanding of what controls IAV infection outcomes at the individual cellular level is still not fully understood (10).

To address this knowledge gap, we conducted a genome-wide CRISPRa screen to define cell intrinsic factors that can antagonize IAV infection. Our screens and subsequent validation identify both appreciated and novel regulators of IAV infection. We further demonstrate that Jade family PHD zinc finger 3 (JADE3), also called PHF16, but not the closely related paralogs JADE1 and JADE2 induces the activation of NF-kB and interferon-induced transmembrane protein 3 (IFITM3) expression and blocks IAV replication. Overall, our results provide new insight into both host-viral conflicts and the function of poorly described host genes that may have implications beyond host-cellular defense.

Results

Genome-wide CRISPRa screen identifies known and novel regulators of IAV infection

To identify human genes with antiviral potential against IAV, we took a gain of function CRISPRa approach similar to our previous screens with murine norovirus (11). Briefly, we

* For correspondence: Robert C. Orchard, Robert.Orchard@UTSouthwestern.edu.

transduced HeLa dCas9-VP64–expressing cells with the Calabrese CRISPRa library (12). These CRISPRa pool of HeLa cells were infected with the H1N1 IAV strain Puerto Rico/8/1934 (PR8) at an multiplicity of infection (MOI) 1.0 in serum-free media in the presence of L-1-tosylamido-2-phenylethyl chloromethyl ketone (TPCK-trypsin) to allow for viral spread (Fig. 1*A*). As a control, cellular pools containing the Calabrese library were mock infected. After 3 days, IAV-infected cultures were washed, and media were replaced with serum-containing media for recovery. Following a 2-day recovery, cells were again infected with IAV for 3 days and the surviving cells were collected. Single guide RNAs (sgRNAs) from resistant cells were compared to mock-infected controls using STARS (13). We consider a gene a hit if the false discovery rate (FDR) was less than 0.25. 22 genes met this criterion (Fig. 1*B*, and Tables S1 and S2).

Upon examination of enriched genes, we identify known antiviral genes toward IAV, including the interferon-stimulated genes (ISGs) *MX1*, *IFITM1*, and *P2RY6* (14–16). *B3GAT1* also was significantly enriched and was recently shown to broadly restrict influenza viruses by decreasing sialic acid levels at the cell surface (17). Other hits include genes encoding the glycan-modifying fructosyltransferases *FUT1* and *FUT4* and a component of the V-ATPase *ATP6V1C1* involved in endosomal acidification, suggesting possible roles for these genes inhibiting viral entry (18–20). Finally, poorly studied genes with no known antiviral role in influenza A infection also showed significant enrichment, including *JADE3* and *LRRC15*. Of these, *LRRC15* has been shown to inhibit SARS-CoV-2 infection and binds spike protein (21–23). When we compare our dataset with a previously conducted CRISPRa IAV screen, we detect only minimal overlap outside of *B4GALNT2*, the most enriched gene in each screen (Fig. S1) (24). This variation in data is likely due to numerous technical differences in the design of the CRISPRa screens. Overall, our screen identifies many pathways and genes appreciated to be important for IAV infection while also suggesting new genes with unknown links to IAV biology.

To validate our screening data, we individually introduced two sgRNAs per gene into HeLa-dCas9-VP64 cells targeting *B4GALNT2*, *ATP6V1C1*, *B3GAT1*, *JADE3*, *FUT4*, *LRRC15*, *DIRC2*, *TMEM150A*, *P2RY1*, and *P2RY6* and compared them to cells transduced with either an empty sgRNA plasmid or an sgRNA-targeting *CD4*. We confirmed that each guide increased gene expression of the respective target gene (Fig. 2*A*). We next challenged these cell lines with an IAV PR8

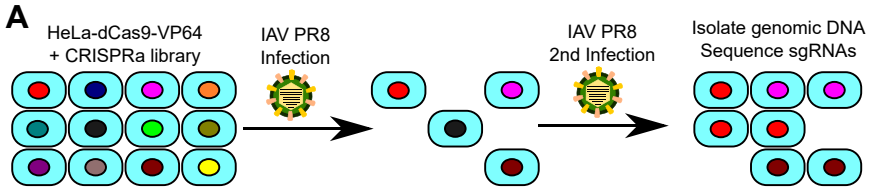

B

Gene Symbol	STARS Score	p-value	FDR
B4GALNT2	20.40	<1.23e-6	<1.34e-3
ATP6V1C1	15.39	<1.23e-6	<1.34e-3
B3GAT1	10.12	<1.23e-6	<1.34e-3
JADE3	8.47	<1.23e-6	<1.34e-3
FUT4	8.05	<1.23e-6	<1.34e-3
LRRC15	7.43	<1.23e-6	<1.34e-3
FUT1	6.79	<1.23e-6	<1.34e-3
CHST1	6.37	<1.23e-6	<1.34e-3
DIRC2	6.24	<1.23e-6	<1.34e-3
B3GNT6	5.77	1.23e-5	<1.33e-2
MX1	5.66	1.60e-5	<1.43e-2
SOX17	5.67	2.21e-5	<1.81e-2
IFITM1	5.43	2.83e-5	0.021
CTSL	5.28	4.43e-5	0.031
ITGB5	5.01	9.59e-5	0.062
TMEM150A	4.82	1.35e-4	0.066
SFN	4.80	1.44e-4	0.067
P2RY1	4.69	1.80e-4	0.080
MKNK2	4.64	1.96e-4	0.083
P2RY6	4.38	3.41e-4	0.139
STARD3	4.28	5.06e-4	0.199
AADAC	4.12	6.30e-4	0.238

Figure 1. Genome-wide CRISPR activation screen identifies antiviral proteins against influenza A virus. *A*, schematic of genome-wide CRISPRa screening strategy to identify antiviral genes for influenza a virus (IAV). Sequences of the sgRNAs from cells surviving IAV challenge were quantified and compared to the relative abundance of a mock-infected sample. *B*, table of significantly enriched genes. STARS algorithm was used to calculate STARS score, *p*-value, and false discovery rate (FDR). Genes colored in *blue* have previously been shown to possess anti-IAV activity. FDR scores are shown and color coded for <0.01 (*yellow*), <0.05 (*orange*), and <0.25 (*gold*). JADE3 (*bolded*) was chosen for additional validation. JADE3, Jade family PHD zinc finger 3; sgRNA, single guide RNA.

A

Gene	Guide	Average RNA Change
B4GALNT2	A	68,700 Fold
B4GALNT2	B	8,250 Fold
ATP6V1C1	A	9.6 Fold
ATP6V1C1	B	26 Fold
B3GAT1	A	569,473 Fold
B3GAT1	B	232,385 Fold
JADE3	A	22 Fold
JADE3	B	19 Fold
FUT4	A	15 Fold
FUT4	B	4 Fold
LRRC15	A	927 Fold
LRRC15	B	839 Fold
DIRC2	A	268 Fold
DIRC2	B	246 Fold
TMEM150A	A	9,444 Fold
TMEM150A	B	25,242 Fold
P2RY1	A	741 Fold
P2RY1	B	1,180 Fold
P2RY6	A	43 Fold
P2RY6	B	32 Fold

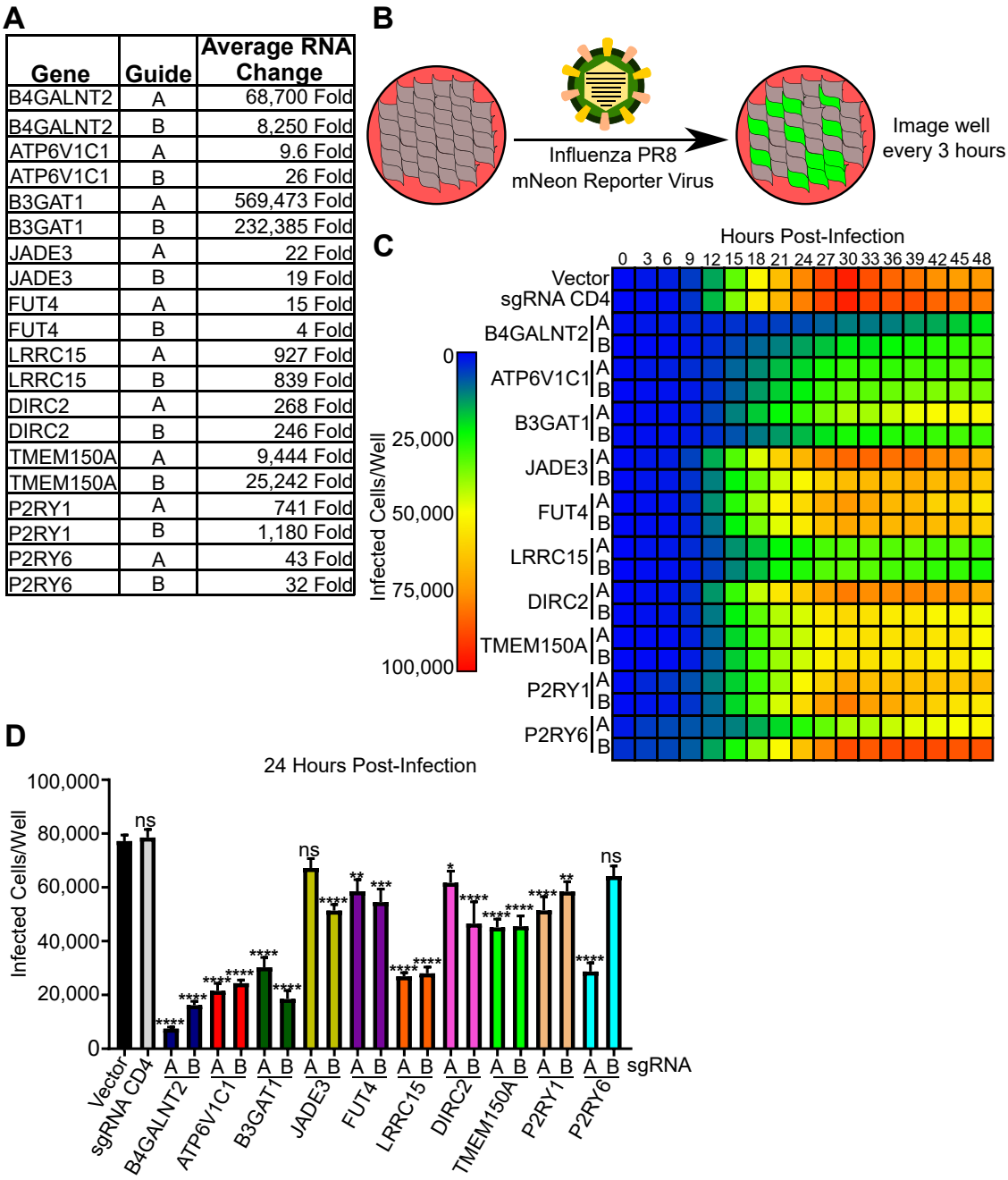

Figure 2. Validation of CRISPR activation screen. *A*, table showing mRNA fold change of indicated gene in HeLa-dCas9 VP64 cells expressing guides (*A*) or (*B*) to the indicated gene. Data is shown as the average of three independent experiments. *B*, *cartoon schematic* of the validation assay in which HeLa-dCas9 VP64 cells were infected with PR8 mNeon reporter virus and mNeon fluorescence was monitored every 3 h *via* IncuCyte. *C*, heat map displaying the number of infected cells per well over a 48 h time course for each cell line expressing the indicated sgRNA construct. Data is the average from three independent experiments. *D*, number of cells infected with influenza PR8 mNeon at 24 h postinfection from (*C*). The data are shown as means ± the SEM from three independent experiments, and data were analyzed for statistical differences for each cell line compared to the vector control by one-way ANOVA with Tukey's multiple-comparison test. *$p < 0.05$; **$p < 0.01$; ***$p < 0.001$; and ****$p < 0.0001$. ns, not significant; PR8, Puerto Rico/8/1934; sgRNA, single guide RNA.

strain expressing mNeon as a reporter (25). Infection was monitored for 48 h by quantifying mNeon expression in each well every 3 h (Fig. 2*B*). Of the ten genes tested, all ten showed antiviral activity with at least one of the two guides and eight genes had both sgRNAs display significant antiviral activity toward mNeon reporter IAV at 24 h postinfection (Fig. 2, *C* and *D*). The presence of well-known antiviral genes amongst our enriched genes and the independent validation provides confidence that our screening dataset is robust.

JADE3 is sufficient and necessary to inhibit influenza A infection

Of the enriched genes with unappreciated antiviral function, *JADE3* also demonstrated antiviral activity in a recent CRISPRa screen for SARS-CoV-2 in Calu-3 cells and murine norovirus in HeLa cells (11, 26). Together these findings suggest the antiviral activity of JADE3 is not cell-type or virus-specific. *JADE3* is a poorly studied member of the Jade family of proteins consisting of JADE1, JADE2, and JADE3. Jade

family members are believed to have mostly redundant roles in the histone acetyltransferase histone acetyltransferase binding to ORC1 (HBO1) complex and have been predominantly studied for their role in cancer and development (27, 28). More specifically, the Jade family proteins direct the complex to histone H4 acetylation, which regulates gene transcription (29, 30). Phylogenetic analysis shows distinct orthologs for all three JADE proteins extending back to jawed vertebrates (Fig. 3*A*). However, while two JADE-like proteins exist in the jawless vertebrate lamprey, they do not cluster with any of the three JADE proteins, suggesting significant amino-acid replacements during the jawed-jawless divide in vertebrates. Since this divide coincides with the expansion of the immune system, we hypothesized JADE3 may have a role in the immune system (31). Because of its novelty, its potential broad viral inhibition, and its evolutionary history, we selected *JADE3* for further study.

To determine whether *JADE3* is able to inhibit a non-reporter IAV infection, we generated A549 cells stably overexpressing a *JADE3* complementary DNA (cDNA) with a C-terminal 3xFLAG epitope (Fig. 3*B*). A549 cells are a lung epithelial carcinoma cell line commonly used to study IAV infection (32). A549-JADE3 cells produced less virus after 24 h compared to A549-vector control cells (Fig. 3*C*). Next, we sought to determine the necessity of JADE3 for viral inhibition. Using CRISPR-Cas9, we generated single cell clones with indels in exon 5 of *JADE3,* leading to premature stop codons (Figs. 3*D* and S2). A549ΔJADE3 cells had a modest increase in viral titers 24 h postinfection with IAV (Fig. 3*E*). Complementation with JADE3 cDNA restored IAV titers to levels comparable with the parental cell line, confirming the on-target activity of the sgRNAs (Fig. 3, *F* and *G*). Taken together these data indicate that JADE3 is both necessary and sufficient to optimally inhibit IAV.

The Jade family members JADE1 and JADE2 are not sufficient to inhibit influenza A infection

JADE3 is an 823 amino acid long protein that contains two mid-molecule plant homeodomains (PHDs, Fig. 4*A*). These zinc finger domains have the capacity for the binding and recognition of histone modifications (33). Deletion of either PHD domains or in combination, abrogated the antiviral activity of JADE3 (Fig. 4*B*). The paralogs JADE2 and JADE1 share significant sequence homology with both of the PHD domains of JADE3 (Fig. S3). However, unlike JADE3, expression of JADE1 or JADE2 is insufficient to reduce IAV titers (Fig. 4, *C* and *D*). While, all Jade family members direct histone acetylation *via* the HBO1 complex thus regulating gene expression, our data suggests nonredundant functions of Jade family members (29, 34, 35).

JADE3 is required for basal and full induction of IFITM3 expression

Since JADE3 is known to function in regulating histone acetylation, we hypothesized that JADE3 antiviral function results from changes in host gene expression. Thus, we conducted RNA-seq of uninfected A549ΔJADE3 cells and A549 WT cells. A549ΔJADE3 cells had a significant (FDR adjusted p value < 0.01) increase in the expression of 1183 genes and a significant decrease in the expression of 1276 genes as compared to WT cells (Fig. 5*A* and Table S3A). Many antiviral effectors are ISGs, so named because their expression is robustly induced by interferons (IFNs). Many ISGs are also direct targets of other signaling pathways and can be induced in the absence of IFN or are expressed at baseline with further induction during a response (36). Since a large portion of the cell intrinsic antiviral response acts through ISGs, we examined the expression of ISGs in A549ΔJADE3 cells and A549 WT cells (Fig. 5*B*). Surprisingly, we find most ISGs are increased in A549ΔJADE3 cells. A notable exception is IFITM3, which shows a 3-fold reduction. IFITM3 is a well-studied antiviral molecule important for restriction of influenza entry *in vitro* and *in vivo* (14, 37). Polymorphisms in IFITM3 are associated with higher risk of IAV infection and hospitalization in humans (38). Unlike many ISGs, IFITM3 is expressed at basal levels in some cell types and this basal level is sufficient to inhibit infection (39, 40). We find A549 cells lacking JADE3 have decreased mRNA expression of IFITM3 and this effect is partially rescued by complementation back of a JADE3 cDNA (Fig. 5, *C* and *D*). This effect is maintained or more pronounced in the setting of IAV infection or tumor necrosis factor (TNF)-α stimulation (Fig. 5, *C* and *D*). Interestingly, the difference is more subtle with IFN-β stimulation (Fig. 5, *C* and *D*). Protein levels of IFITM3 are congruent, with decreased protein levels in cells lacking JADE3 and a partial rescue by complementation both at baseline and during influenza infection (Fig. 5*E*). Therefore, these data indicate that the basal expression and the induction of IFITM3 by danger signals is regulated by JADE3.

JADE3 activates expression of a TNF genetic program

The functional differences between Jade family members have greatly been understudied. Thus, we set out to define different gene expression patterns in A549 cells expressing either a vector control, JADE3, or JADE2. Principal component analysis demonstrates significant gene expression changes when either JADE3 or JADE2 is overexpressed (Fig. 6*A*). Importantly, JADE3 and JADE2 samples form distinct clusters, demonstrating unique expression patterns. We hypothesized that JADE3 induces an antiviral gene expression profile including IFITM3 that is distinct from JADE2. To this end we compared the differentially expressed genes from both JADE2 and JADE3 relative to vector control cells. JADE3 overexpression caused significant (FDR adjusted p value < 0.01) upregulation of 1155 genes and downregulation of 1124 genes as compared to a vector control (Fig. 6*B* and Tables S3, B and E). JADE2 overexpression caused significant upregulation of 829 genes and downregulation of 816 genes as compared to a vector control (Tables S3, C and D). Furthermore, 716 genes were uniquely upregulated in JADE3-expressing cells and not in JADE2-expressing cells, suggesting differing roles for the two JADE proteins (Fig. 6*C*). Surprisingly, neither of the JADE proteins significantly altered IFITM3 expression suggesting

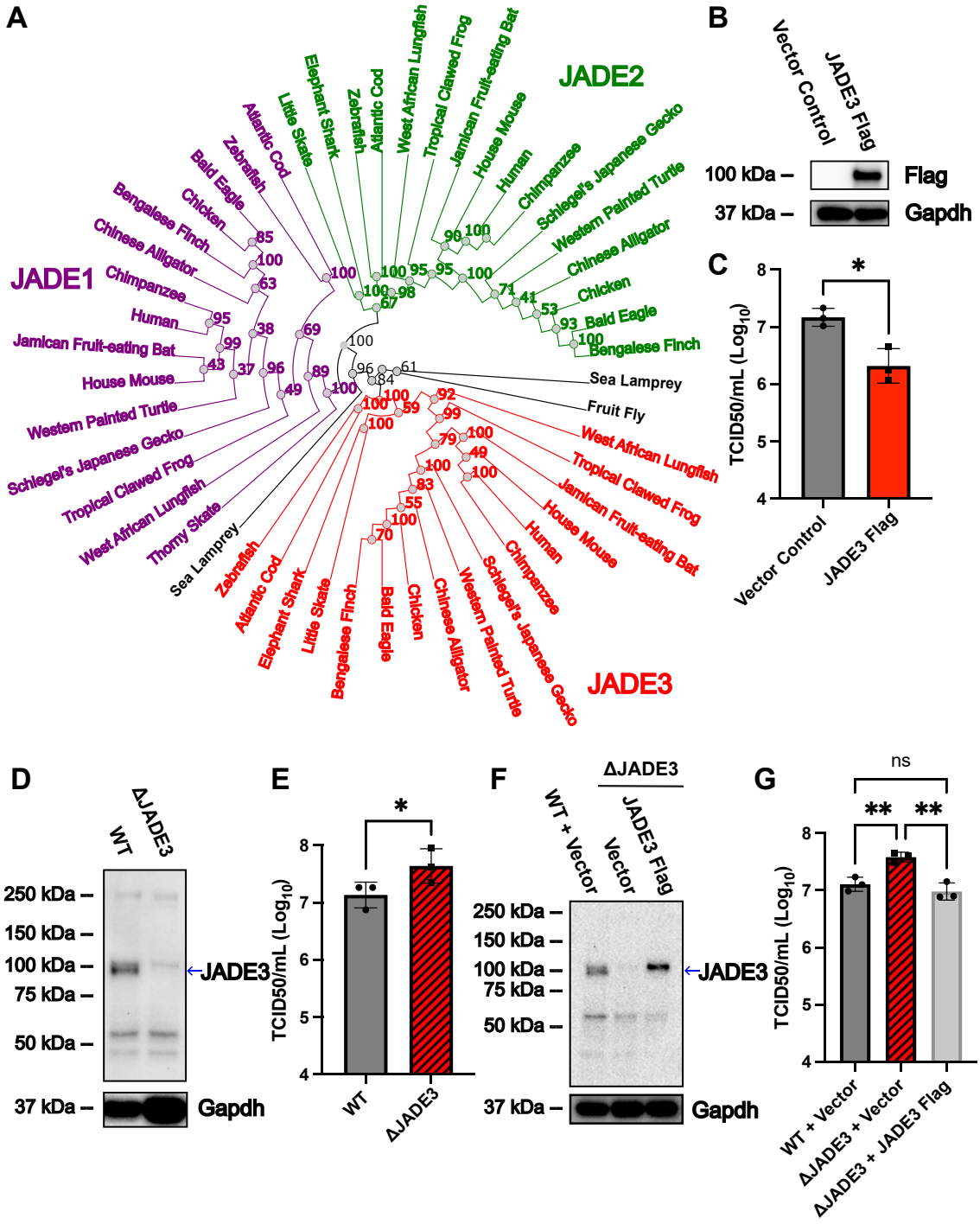

Figure 3. JADE3 is sufficient and necessary to restrict influenza A infection. *A*, maximum likelihood phylogenetic tree of JADE3 orthologs. One hundred bootstrap replicates were performed and bootstrap values are indicated. Branch length represents amino acid changes per site. GenBank common names are used for species. Ortholog gene groups for JADE3 (*red*), JADE1 (*purple*), and JADE2 (*green*) are colored. Potential JADE orthologs that do not branch with one of the three JADE proteins are in *black*. *B*, representative Western blot from three experiments of JADE3 Flag expression from control and JADE3 Flag transduced A549 cells. *C*, vector control or JADE3 Flag A549 cells were challenged with WT PR8 at a MOI of 0.01. Infectious virus titer was determined by TCID50 24 h postinfection. Data was analyzed using a paired two-tail *t* test. *D*, representative Western blot from three experiments for JADE3 expression in indicated cell lines. *Blue arrow* indicates expected molecular weight of JADE3. *E*, A549 WT or A549ΔJADE3 cells were challenged with WT PR8 at a MOI of 0.01. Infectious virus titer was determined by TCID50 24 h postinfection. Data was analyzed using a paired two-tail *t* test. *F*, representative Western blot from three experiments for JADE3 expression in indicated cell lines. *Blue arrow* indicates expected molecular weight of JADE3. *G*, A549 control or A549ΔJADE3 cells complemented with either a vector control or JADE3 were challenged with WT PR8 at a MOI of 0.01. Infectious virus titer was determined by TCID50 24 h postinfection. Data was analyzed using a one-way ANOVA with Tukey's multiple comparisons test. All data shown is mean ± SD from three independent experiments. *$p < 0.05$ and **$p < 0.01$. JADE3, Jade family PHD zinc finger 3; MOI, multiplicity of infection; ns, not significant; PR8, Puerto Rico/8/1934.

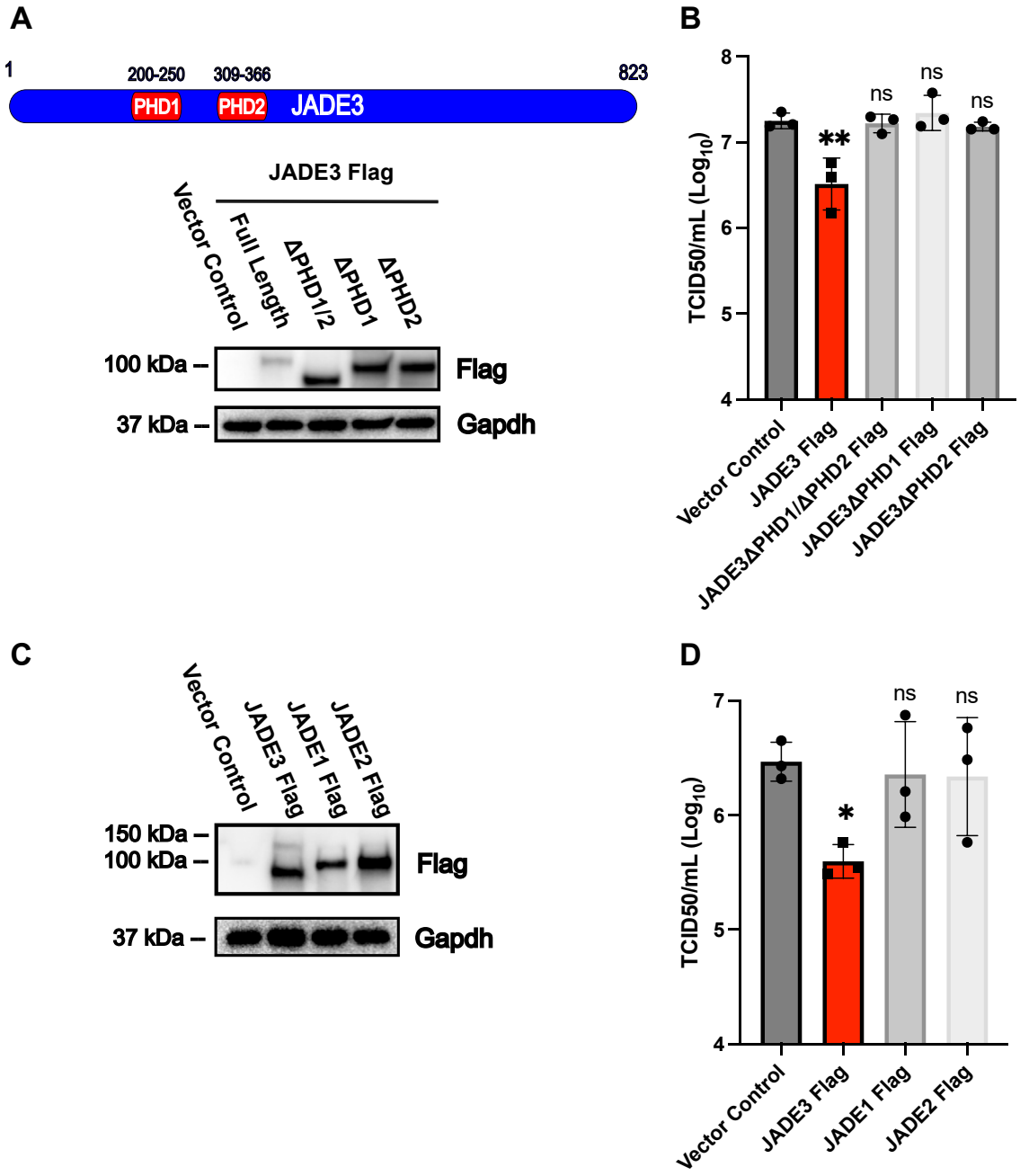

Figure 4. Analysis of JADE3 domains and paralogs antiviral function. *A*, achematic of JADE3 and its PHDs. Representative Western blot from three experiments of A549 cells transduced with a vector control, JADE3 Flag, or JADE3 lacking both or either PHDs. *B*, A549 cells expressing either a vector control or the indicated PHD truncations were challenged with WT PR8 at a MOI of 0.01. Infectious virus titer was determined by TCID50 24 h postinfection. *C*, representative Western blot from three experiments of expression of flag tagged JADE1, JADE2, JADE3 in A549 cells. *D*, A549 cells expressing different Jade family proteins were challenged with WT PR8 at a MOI of 0.01. Infectious virus titer was determined by TCID50 24 h postinfection. All data shown is mean ± SD from three independent experiments. Data was analyzed using a one-way ANOVA with Dunnett's multiple comparisons test against the vector control. *$p < 0.05$ and **$p < 0.01$. JADE3, Jade family PHD zinc finger 3; MOI, multiplicity of infection; ns, not significant; PHD, plant homeodomain; PR8, Puerto Rico/8/1934.

that while JADE3 is required for IFITM3 expression, JADE3 overexpression is not sufficient to significantly increase IFITM3 mRNA at baseline (Tables S3, B and C). Thus, we hypothesized that JADE3 may require a stimulus or other factor to increase IFITM3 expression. Such a factor would have a gene signature enriched in genes both depleted in JADE3 KO cells and increased in JADE3 overexpression cells. To identify pathways that might augment IFITM3 expression in the context of JADE3, we conducted a gene set enrichment analysis of such genes, which showed significant upregulation of the TNF/NF-kB pathway (Fig. 6*D*). While genes upregulated in A549ΔJADE3 cells have some enrichment of TNF/NF-kB pathway genes, the pathway is notably more enriched in the 500 most significantly increased genes in JADE3-expressing cells (Figs 6*E*, S4, S5, and S6). Since the TNF/NF-kB pathway was one of the most enriched and TNF treatment

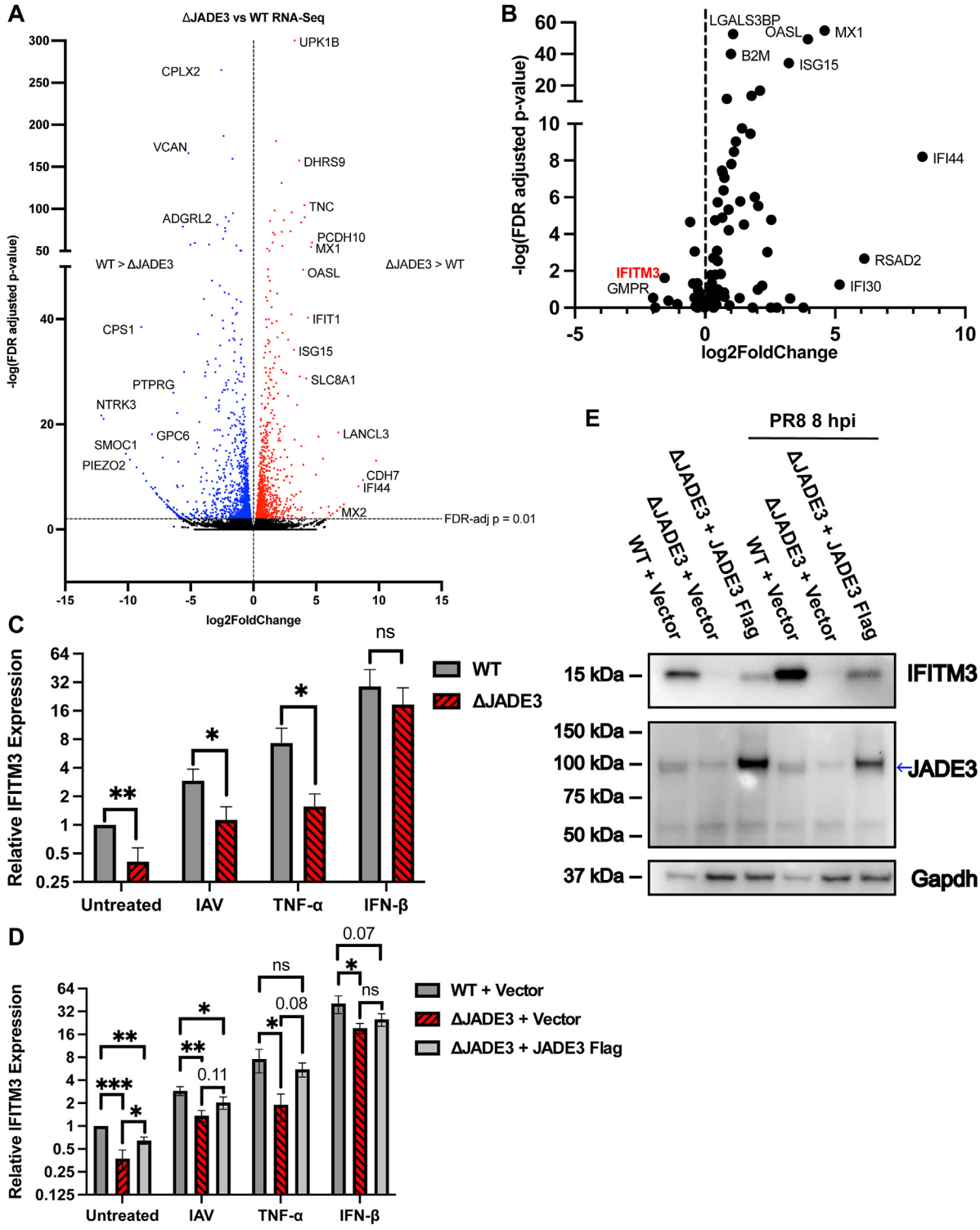

Figure 5. JADE3 is required for basal and inducible IFITM3 expression. *A*, *volcano plot* of RNA-seq of A549ΔJADE3 cells *versus* WT cells. An FDR adjusted *p* value <0.01 (*dotted line*) was considered significant. Data is from three biological replicates. *B*, *scatter plot* of ISGs from RNA-seq of A549ΔJADE3 cells *versus* WT cells. Data is from three biological replicates. IFITM3 is shown in *red*. *C*, A549 WT or A549ΔJADE3 cells were either challenged or treated with the labeled condition and IFITM3 mRNA expression was measure by qPCR. Expression was normalized to actin. IAV challenge was done at a MOI of 3 for 8 h. TNF-α and IFN-β treatment was done for 6 h. Data shown is from three independent experiments presented as mean ± SD relative fold change compared to untreated vector control. Data was analyzed using independent two-tail *t* test for each condition. *D*, A549 vector control, A549ΔJADE3 complemented with a vector control, or A549ΔJADE3 complemented with JADE3 were either challenged or treated with the labeled condition and IFITM3 mRNA expression was measure by qPCR. Expression was normalized to actin. IAV challenge was done at a MOI of 3 for 8 h. TNF-α and IFN-β treatment was done for 6 h. Data shown is from three independent experiments presented as mean ± SD relative fold change compared to untreated vector control. Data was analyzed using independent one-way ANOVAs with Tukey's multiple comparisons test for each condition. *E*, A549 control cells and A549ΔJADE3 cells complemented with either a vector control or JADE3 Flag were challenged with WT PR8 at a MOI of 3. Whole-cell lysis was extracted 8 h postinfection and resolved using SDS-PAGE and probed for IFITM3. Western blot shown is representative of three experiments. *$p < 0.05$ and **$p < 0.01$. FDR, false discovery rate; IAV, influenza A virus; IFITM3, interferon-induced transmembrane protein 3; JADE3, Jade family PHD zinc finger 3; MOI, multiplicity of infection; ns, not significant; qPCR, quantitative PCR; TNF, tumor necrosis factor.

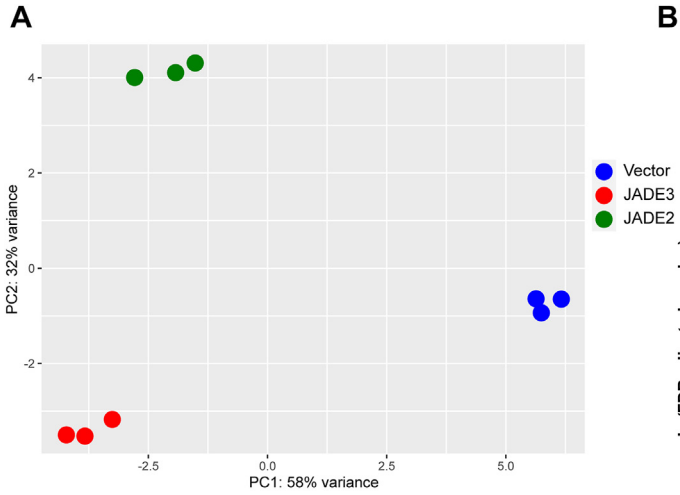

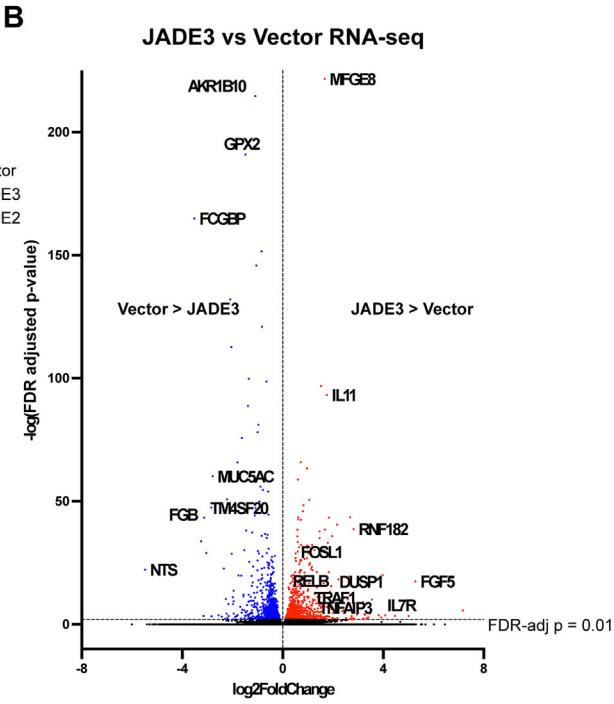

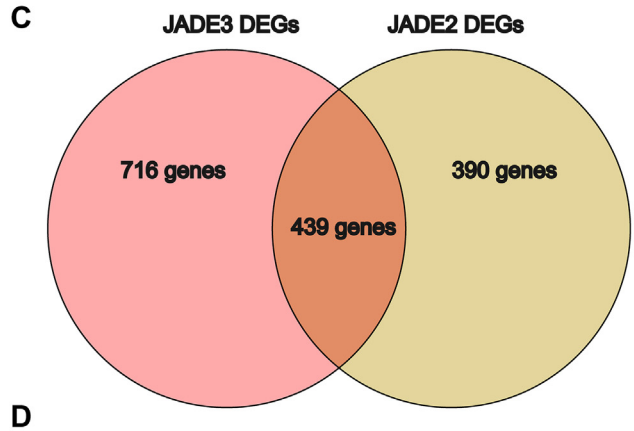

D

Decreased in ΔJADE3 and increased in JADE3 Flag

Gene set (number of genes in set)	Number of genes in overlap	p-value	FDR q-value
Hallmark epithelial mesenchymal transition (200)	16	1.27E-11	6.34E-10
Hallmark MYC targets (200)	12	1.17E-7	2.96E-6
Hallmark E2F targets (200)	11	9.34E-7	1.17E-5
Hallmark TNFa signaling via NF-kB (200)	11	9.34E-7	1.17E-5
Hallmark apical junction (200)	10	6.80E-6	4.25E-5
Hallmark estrogen response early (200)	10	6.80E-6	4.25E-5
Hallmark hypoxia (200)	10	6.80E-6	4.25E-5
Hallmark myogenesis (200)	10	6.80E-6	4.25E-5
Hallmark G2M checkpoint (200)	9	4.48E-5	2.49E-4
Hallmark DNA repair (150)	7	2.52E-4	1.26E-3

E

Upregulated in JADE3 Flag

Gene set (number of genes in set)	Number of genes in overlap	p-value	FDR q-value
Hallmark epithelial mesenchymal transition (200)	45	4.07E-44	2.04E-42
Hallmark TNFa signaling via NF-kB (200)	44	1.09E-42	2.72E-41
Hallmark hypoxia (200)	31	1.83E-25	3.06E-24
Hallmark p53 pathway (200)	24	2.37E-17	2.96E-16
Hallmark apical junction (200)	20	3.64E-13	3.64E-12
Hallmark apoptosis (161)	18	8.15E-13	6.79E-12
Hallmark Inflammatory response (200)	19	3.54E-12	2.53E-11
Hallmark IL2 STAT5 signaling (199)	18	2.99E-11	1.62E-10
Hallmark glycolysis (200)	18	3.25E-11	1.62E-10
Hallmark KRAS signaling (200)	18	3.25E-11	1.62E-10

Figure 6. Transcriptional profiling reveals that JADE3 activates the TNF/NF-kB signaling pathway. *A*, principal component analysis *scatter plot* showing differential gene expression signatures of control, JADE3- or JADE2-expressing cells. PC1 and PC2 corresponding to the principal component 1 and principal component 2. *B*, *volcano plot* of RNA-seq of A549 JADE3 Flag cells *versus* vector control cells. An FDR-adjusted *p*-value < 0.01 (*dotted line*) was considered significant. Data is from three biological replicates. *C*, *Venn diagram* of differentially expressed genes (DEGs) significantly upregulated by JADE3 Flag *versus* vector control and JADE2 Flag *versus* vector control. *D*, gene set enrichment analysis of genes that were both downregulated in ΔJADE3 cells (FDR-adjusted *p* value < 0.05) and upregulated in JADE3 Flag cells (FDR-adjusted *p* value < 0.05). The ten most significantly enriched gene sets are shown. *E*, gene set enrichment analysis of the 500 most significantly upregulated genes in A549 cells expressing either JADE3 Flag or a vector control. The ten most significantly enriched gene sets are shown. FDR, false discovery rate; JADE3, Jade family PHD zinc finger 3; TNF, tumor necrosis factor.

was previously able to induce IFITM3 expression, we decided to explore the possibility that JADE3 regulates IFITM3 expression *via* NF-kB to inhibit IAV infection.

JADE3 expression increases NF-kB translocation to the nucleus and phosphorylation

Focusing on the TNF/NF-kB pathway in JADE3-expressing cells, we found upregulation of canonical genes in the pathway including *RELB*, *TRAF1*, *FOSL1*, *IL6* (Fig. 7*A*). In contrast to JADE3, JADE2 has only modest changes in the expression profile of the TNF/NF-kB pathway. Upon activation, NF-kB translocates to the nucleus where it activates transcription. Furthermore, NF-kB (p65) can be phosphorylated at serine 536, which enhances its transcriptional activity and is used as a marker for active NF-kB (41, 42). Nuclear extracts from JADE3-expressing cells had significant NF-kB p65 protein levels, while it was largely absent from control cells (Fig. 7*B*). JADE3-expressing cells had an increase in serine 536 phosphorylated p65 even after treatment with recombinant human TNF-α (Fig. 7*C*). Consistent with the antiviral activity of JADE3, the increase in phosphorylated p65 by JADE3 requires both PHD domains (Fig. 7*D*). Importantly, expression of the other JADE paralogs is insufficient, with JADE1-expressing cells having no increase in phosphorylated p65, while JADE2-expressing cells have a modest increase in phosphorylated p65, consistent with a moderate increase in some NF-kB pathway genes (Fig. 7*E*).

JADE3 antiviral function requires both NF-kB and IFITM3

NF-kB is a master inflammatory transcription factor that induces expression of a variety of genes, including antiviral genes. Since JADE3 activates NF-kB signaling and is required for proper IFITM3 expression upon TNF-α stimulation, we hypothesized JADE3, NF-kB, and IFITM3 may be linked. Specifically, NF-kB may be required for JADE3's effect on IFITM3 expression and IAV infection. To study this, we used CRISPR-Cas9 to generate two polyclonal knockouts of each NF-kB p65 and IFITM3 in A549 vector control and JADE3-expressing cells (Fig. 8*A*). Probing for IFITM3, we find that while JADE3 expression is able to increase IFITM3 protein levels, this effect is abrogated in NF-kB p65 KO cells (Fig. 8*B*).

Next, we challenged these cells with influenza A and find that while JADE3 expression in control cells is able to significantly inhibit IAV, it is unable to do so in cells lacking p65 (Fig. 8*C*). Furthermore, IFITM3 is also required for JADE3 antiviral function with JADE3 unable to significantly inhibit IAV in either IFITM3 knockouts. In one of these IFITM3 knockouts, viral growth in JADE3-expressing cells trended toward inhibition of IAV, however this knockout had reduced IFITM3 knockout efficiency as evidenced by Western blot, suggesting this may be due to residual IFITM3 expression (Fig. 8*A*). Taken together, our data demonstrates that JADE3 modulates IFITM3 expression in a NF-kB–dependent manner to inhibit influenza A infection (Fig. 9).

Discussion

In this study, we perform a CRISPRa screen and find a novel antiviral factor JADE3 that regulates IFITM3 expression at multiple levels (Fig. 9). First, JADE3 acts through the NF-kB pathway to increase IFITM3 expression at the protein level. This is evidenced by the fact that JADE3 increases IFITM3 protein levels in a NF-kB p65–dependent manner. Second, JADE3 is required for expression of IFITM3 mRNA at baseline and in response to different stimuli, suggesting JADE3 regulates transcription of IFITM3 likely at the chromatin level since JADE3 antiviral function is dependent on both PHD domains. Interestingly, JADE3's effect on IFITM3 mRNA is enhanced with TNF stimulation linking JADE3's activity with the NF-kB pathway.

Here, we conducted a genome-wide CRISPRa screen to identify antiviral factors against IAV. While many CRISPR screens have been conducted to identify host factors involved in viral infection, most have used a loss-of-function approach. Recently, CRISPRa has been leveraged to discover novel antiviral or proviral genes (11, 24, 26, 43–47). This gain-of-function approach is well suited for interrogating the immune system as it enables the inclusion of genes that are essential, redundant, or have compensatory mechanisms. As compared to a previous CRISPRa screen done with IAV, we find little overlap between significantly enriched genes (24). Importantly, our list of 22 potential antiviral genes includes well-known antiviral genes, including ISGs and novel genes with unknown antiviral activity against IAV. Many of the enriched genes encode for enzymes that modify glycans (Fig. 1*B*). Our results add to the growing body of evidence that glycan modification is an effective antiviral strategy against many viruses (17). A limitation of our study is that we did not investigate the function of any of these genes, including JADE3 *in vivo*. Thus, further interrogation of the physiological function of these genes during IAV infection *in vivo* is warranted.

The JADE protein family consists of three highly similar proteins that function in the HBO1 complex to direct histone acetylation (35). This histone acetyltransferase complex is important for bulk H3K14 and H4 acetylation and has largely been investigated in the context of cancer and development (34, 48–50). The complex consists of multiple subunits including one of either JADE1/2/3 or BRPF1/2/3 using their PHD domains to direct the complex (29). Furthermore, the switch from BRPF1/2/3 to JADE1/2/3 changes the specificity of the complex from H3K14 to H4 acetylation (29). To our knowledge, comparison of the function of the three JADE proteins has not been done, and it has been speculated that they have at least partially redundant function (28). In this study, we find a unique phenotype for JADE3-expressing cells. JADE3 but not JADE1 or JADE2 significantly inhibit IAV. While JADE2 and JADE3 share many differentially expressed genes, the majority of differentially expressed genes are uniquely regulated by JADE2 or JADE3 suggesting nonredundant roles for the JADE proteins (Fig. 6*C*). Distinct roles for the JADE proteins are also supported by the phylogenetic analysis, which shows distinct orthologs for each of the JADE proteins extending back to jawed vertebrates.

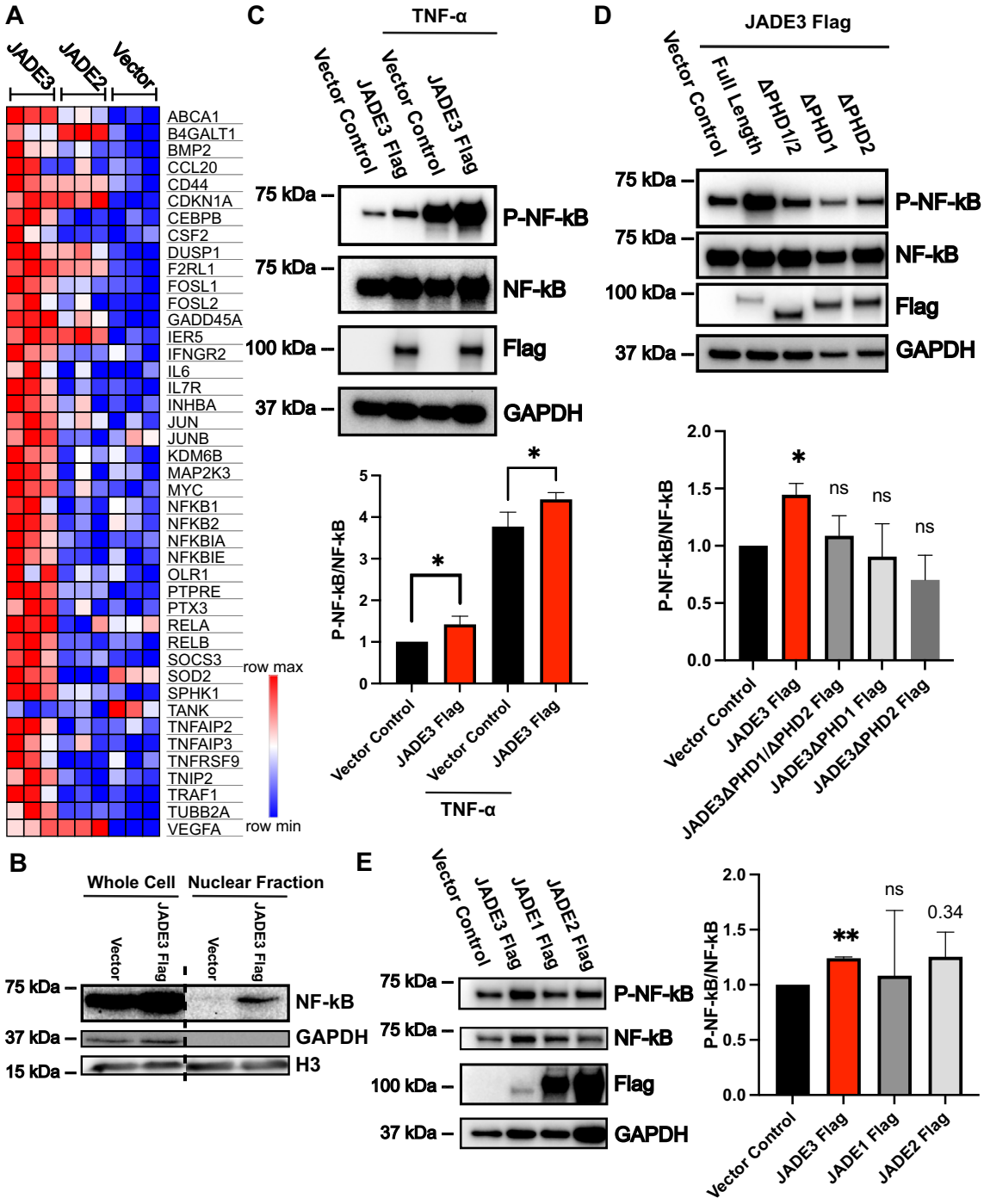

Figure 7. JADE3 expression activates NF-kB p65. *A*, heat map of RNA-seq normalized read count for select genes involved in canonical TNF-α/NF-kB signaling pathway. Coloring is done relative to each row with higher normalized read counts in *red* and lower normalized read counts in *blue*. Each box is one biological replicate. *B*, vector control or JADE3 Flag A549 cells were lysed and nuclei were fractionated. Whole-cell lysis and nuclear fractions were resolved using SDS-PAGE and probed for NF-kB p65. Image was spliced at *dashed line* from a single blot. Western blot shown is representative of three experiments. *C*, *top*: vector control or JADE3 Flag A549 cells were treated with 20 ng/ml of TNF-α for 15 min and then lysed. Whole cell-lysis was resolved using SDS-PAGE and probed for phosphorylated NF-kB p65 (serine 536). Western blot shown is representative of three experiments. *Bottom*: P-NF-kB band intensity was quantified and normalized to NF-kB band intensity. Data shown is from three experiments presented as mean ± SD relative fold change compared to vector control. Data was analyzed using independent two-tail *t* tests. *D*, *top*: whole-cell lysis from A549 cells expressing either vector control, JADE3 Flag, or JADE3 Flag lacking the indicated PHDs were resolved using SDS-PAGE and probed for phosphorylated NF-kB p65 (serine 536). Western blot shown is representative of three experiments. *Bottom*: P-NF-kB band intensity was quantified and normalized to NF-kB band intensity. Data shown is from three experiments presented as mean ± SD relative fold change compared to vector control. Data was analyzed using a one-way ANOVA with Dunnett's multiple comparisons test. *E*, *left*: whole-cell lysis from A549 cells expressing either a vector control or indicated JADE family members were resolved using SDS-PAGE and probed for phosphorylated NF-kB p65 (serine 536). Western blot shown is representative of three experiments. *Right*: P-NF-kB band intensity was quantified and normalized to NF-kB band intensity. Data shown is from three experiments presented as mean ± SD relative fold change compared to vector control. Data was analyzed using a one-way ANOVA with Dunnett's multiple comparisons test. $*p < 0.05$ and $**p < 0.01$. JADE3, Jade family PHD zinc finger 3; ns, not significant; PHD, plant homeodomain; TNF, tumor necrosis factor.

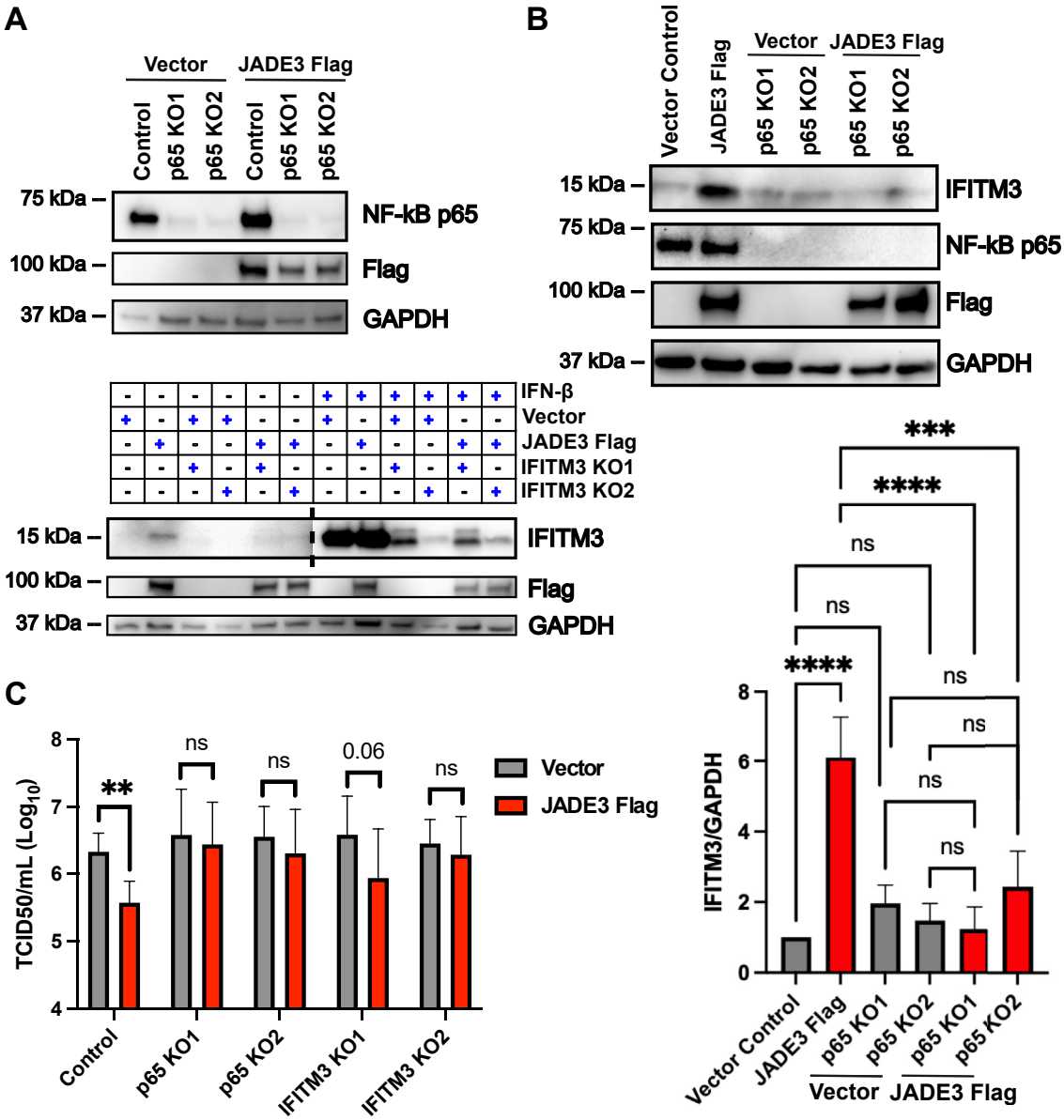

Figure 8. JADE3 antiviral function requires both NF-kB p65 and IFITM3. *A*, *top*: whole-cell lysis from A549 vector control or JADE3-expressing cells transduced with CRISPR/Cas9 to edit NF-kB p65 were resolved using SDS-PAGE and probed for NF-kB P65. KO1 and KO2 denote two unique single guide RNAs used to generate the polyclonal cell lines. Western blot shown is representative of three experiments. *Bottom*: whole-cell lysis from untreated or 24 h IFN-β–treated A549 vector control or JADE3-expressing cells transduced with CRISPR/Cas9 constructs to edit IFITM3 were resolved using SDS-PAGE and probed for IFITM3. KO1 and KO2 denote two separate polyclonal cell lines expressing individual guides targeting IFITM3. *Dashed line* denotes location of splicing of two different exposures of the same blot. Western blot shown is representative of three experiments. *B*, *top*: whole-cell lysis from A549 vector control or JADE3-expressing cells lacking NF-kB p65 expression were resolved using SDS-PAGE and probed for IFITM3. Western blot shown is representative of three experiments. *Bottom*: IFITM3 band intensity was quantified and normalized to GAPDH band intensity. Data shown is from three experiments presented as mean ± SD relative fold change compared to vector control. Data was analyzed using a one-way ANOVA with Tukey's multiple comparisons test. *C*, A549 vector control or JADE3-Flag cells lacking expression of either NF-kB p65 or IFITM3 were challenged with WT PR8 at a multiplicity of infection of 0.01. Infectious virus titer was determined by TCID50 24 h postinfection. Data shown is mean ± SD from three independent experiments and was analyzed using independent paired two-tail *t* tests for each knockout. *$p < 0.05$; **$p < 0.01$; ***$p < 0.001$; and ****$p < 0.0001$. IFITM3, interferon-induced transmembrane protein 3; IFN, interferon; PR8, Puerto Rico/8/1934; JADE3, Jade family PHD zinc finger 3; ns, not significant.

We discover that a remarkable number of genes are transcriptionally regulated by JADE3 suggesting that JADE proteins are global regulators of gene expression (Figs. 5*A* and 6, *A*, and *B*). Thus, it is likely that the antiviral state induced by JADE3 is due to an aggregate of the differential expression of so many genes. However, we are able to determine antiviral function is largely dependent on IFITM3 and NF-kB (Fig. 8*C*). IFITM3 is a well-studied innate immunity protein with potent inhibition of influenza as well as many other viruses (37, 51, 52). Mechanistically, IFITM3 functions to inhibit viral entry by blocking membrane fusion (52–55). IFITM3 expression is robustly activated by IFNs; however, our data suggests that JADE3 is required for expression of IFITM3 independent of IFN. In fact, JADE3 KO cells show activation of the IFN pathway and expression of many canonical ISGs like ISG15 and MX1 but decreased expression of IFITM3 (Fig. 5*B*).

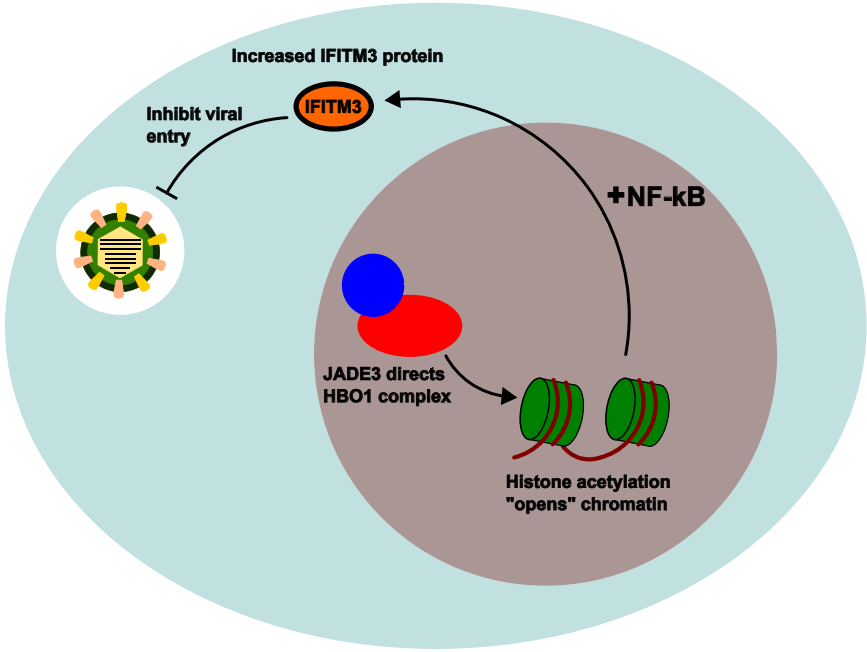

Figure 9. Model of JADE3 antiviral activity through NF-Kb dependent IFITM3 expression. A schematic model of the proposed mechanism for JADE3 antiviral function. JADE3 directs the HBO1 complex to target chromatin. Histone acetylation "opens" chromatin allowing for transcription of target genes. Increased IFITM3 expression in a NF-Kb–dependent manner. IFITM3 inhibits viral entry. HBO1, histone acetyltransferase binding to ORC1; IFITM3, interferon-induced transmembrane protein 3; JADE3, Jade family PHD zinc finger 3.

Increased expression of these other antiinfluenza ISGs may contribute to the smaller phenotype of JADE3 KO cells during infection. Unlike many ISGs, basal expression of IFITM3 has been shown to be important to prevent infection in different cell types, including stem cells (39, 40). We find JADE3 is required for basal IFITM3 expression in A549 cells and may play a role in other cell types upon further investigation.

NF-kB is a central inflammatory transcription factor that has been heavily studied for its role in inflammatory disease, cancer, and infection (56). NF-kB functions in both innate and adaptive immunity bridging the transition between the two arms of the immune system and exerting its effects on a variety of cell types, including lymphocytes and macrophages (57). JADE3 expression is elevated in B cells and due to its evolutionary history, it is possible the protein also plays a role in the adaptive immune system (58, 59) (https://www.proteinatlas.org/ENSG00000102221-JADE3/immune+cell). Owing to its importance in viral infection many viruses either co-opt the NF-kB pathway or inhibit it to support infection (60–63). This includes IAV with NS1 known to modulate NF-kB signaling as well as inhibiting IFITM3 expression (64–66). Furthermore, overactivation of the pathway has been implicated in the pathogenesis of multiple viruses, where damage is often due to over-active inflammatory host damage (67). The increased expression of many NF-kB–related genes in JADE3 overexpression and JADE3 KO cells suggests a complicated balancing of NF-kB signaling by JADE3. Thus, the role of JADE3 during infection with other IAV strains including those that lack NF-kB modulation due to truncations in the viral protein NS1 merits further (64). This is especially important given that NF-kB has been shown to have both antiviral and proviral roles, including in the context of IAV infection (68–70). Alternatively, prior evidence shows IFITM3 functions in a feedback loop to inhibit both IFN and NF-kB signaling potentially explaining the activation of NF-kB in JADE3 KO cells (71, 72). JADE3's activation of NF-kB signaling was dependent on its PHD domains, suggesting its role in chromatin regulation is required (Fig. 7*D*). However, the molecular mechanism by which JADE3 regulates the NF-kB pathway remains an open question. Furthermore, our identification of JADE3 and many of our experiments rely on overexpression of JADE3 in immortalized cell lines. Thus, further studies are required to determine whether they reflect the physiological role of JADE3 in primary cells or *in vivo*.

Despite its centrality to numerous diseases, many of the genes involved in the immune system are not understood. As one of the natural stimuli for the immune system, viruses can help uncover functionally relevant genes involved in inflammation. Indeed, our study couples the powerful genetic selection viruses exert on host cells with an unbiased genetic screen to assign a functional role to a poorly described human gene with relevance beyond antiviral defense.

Experimental procedures

Tissue culture

293T, A549, HeLa, and Madin-Darby canine kidney cells were obtained from American Type Culture Collection and cultured in Dulbecco's modified Eagle's medium supplemented with 5% fetal bovine serum. Cells were routinely screened for *mycoplasma* contamination. To generate stable cell lines, cells were transduced with lentivirus generated by

transfecting lentiviral vectors with psPAX2 and pCMV-VSV-G into 293Ts. After 48 h, supernatants were collected and filtered through a 0.45-μm pore size filter (Millipore) and added to the respective cells. After 48 h, cells were selected with either puromycin or blasticidin.

To generate A549ΔJADE3 cells, two guide RNAs (sgRNAs: ACGTTCTGTTTATCCGACCC, CCGCTATGACCTAGATGACA) targeting exon 5 of JADE3 were formed using CRISPR RNA and trans-activating CRISPR RNA from Integrated DNA Technologies, Inc. Guide RNAs were then complexed with Cas9 nuclease and transfected into A549 cells using lipofectamine CRISPRmax (Invitrogen). Cells were then diluted and plated as single cells. Single cell colonies were grown and validated using Sanger sequencing for indels resulting in premature stop codons. To generate polyclonal knockouts of p65 (KO1 guide: CCTTTCCTACAAGCTCGTGG, KO2 guide: GGAAGATCTCATCCCCACCG) and IFITM3 (KO1 guide: GATGCTCAAGGAGGAGCACG, KO2 guide: GTGGATCACGGTGGACGTCG), the lentiCRISPRv2 system was used (73). After lentivirus transduction and selection, stable cell lines were validated for knockout using immunoblotting for the respective proteins.

Plasmids

Lenti dCas9-VP64 plasmid (Addgene #61425) was used for CRIPSRa. For validation of the screen guides were cloned into pxPR_502 (Addgene #96923). Human JADE3 (accession no. NP_055550.1), JADE2 (accession no. NP_001276913.1), and JADE1 (accession no. NP_001274369.1) cDNAs corresponding to their protein sequences were cloned with C-terminal 3XFlag tags into pCDH-MCS-T2A-Puro-MSCV (Systems Biosciences, CD522A-1). JADE3 constructs lacking the PHD domains were generated using splicing by overlap extension PCR with PHD1 corresponding to amino acids 200 to 250 and PHD2 corresponding to amino acids 309 to 366 and cloned into pCDH-MCS-T2A-Puro-MSCV. To generate polyclonal knockouts, guides were cloned into CRISPRv2 Blast plasmid (Addgene #83480). All plasmids were sequence verified prior to use.

Influenza virus assays

A/PR/8/34 was a kind gift of Herbert Virgin (Washington University). mNeon-PR8 has previously been described (25). For PR8 infection, cells were seeded at 100,000 cells per well in a 24-well plate and incubated overnight in culture media. Next day cells were washed with PBS and infected with virus in virus production serum-free media (VPSFM; Gibco) supplemented with 0.25 to 0.5 μg/ml TPCK-trypsin. At specified time points samples were frozen at −80 °C.

To determine TCID50, Madin-Darby canine kidney cells were seeded 25,000 cells per well in a 96-well plate and incubated overnight. Next day, cells were washed with Dulbecco's Phosphate Buffered Saline and media changed to Dulbecco's modified Eagle's medium + 0.2% bovine serum albumin supplemented with 1.8 to 2 μg/ml TPCK. Cells were infected with serial dilutions of virus samples in replicates and incubated. After CPE was observed (about 3–5 days after infection), plates were fixed with a 4% paraformaldehyde solution, stained with crystal violet, and scored. TCID50/ml was calculated using Reed-Muench method (74).

CRISPRa screen

CRISPRa screen was performed similar to what we have previously reported (11). Briefly, HeLa-dCas9-VP64 cells were transduced with SetA and SetB of the Calabrese CRISPRa library at an MOI of 0.3. Each Calabrese pool was delivered by lentiviral transduction of 1.2×10^8 HeLa cells at an MOI of 0.3. This equates to 3.6×10^7 transduced cells, which is sufficient for the integration of each sgRNA at least 500 independent times. At 2 days posttransduction, puromycin was added to the media, and transduced cells were selected for a total of 7 days. A total of 5×10^6 HeLa CRISPRa cells were seeded in a T-175 tissue culture flask, and each experimental condition was evaluated in duplicate with six independent flasks per replicate (3×10^7 cells per replicate). After seeding cells overnight, media was changed to VPSFM containing 0.5 μg/ml TPCK-trypsin. Cells either left in TPCK-trypsin–containing media or infected with PR8 at an MOI of 1.0 for 48 h. Two days postinfection, mock-infected cells were harvested for genomic DNA extraction. At this time point, roughly 50% of the PR8-infected cells displayed CPE, and cells were washed twice with PBS, and serum-containing media was added. After 2 days of recovery, cells were again challenged with an additional infection of PR8 at an MOI of 1.0 for 48 h. Two days after rechallenge, and cells were washed twice with PBS, and serum-containing media was added for an addition 3 to 5 days prior to harvesting. All flasks from a replicate were harvested together. Genomic DNA was isolated from surviving cells using a QIAamp DNA minikit according to the manufacturer's instructions (Qiagen). Illumina sequencing and STARS analysis were performed as described previously (11).

Validation

HeLa-dCas9 VP64 cells were transduced with lentiviruses expressing CRISPRa sgRNAs for the indicated genes (Fig. S7). Transcriptional activation was confirmed *via* quantitative PCR (qPCR) for the corresponding gene. Briefly, RNA was extracted using a Direct-zol kit (Zymo Research) and cDNA prepared using a high-capacity cDNA reverse transcription kit (Thermo Fisher Scientific). qPCR was performed using primers and probes from IDT (Fig. S8). Expression was normalized relative to the mRNA expression of actin. Cells were then seeded 100,000 cells per well in a 24-well plate and incubated overnight. Cells were then washed and infected with PR8 mNeon virus in VPSFM supplemented with 0.5 μg/ml of TPCK-trypsin. Cells were then incubated in the Incucyte live-cell analysis instrument (Sartorius), and green fluorescence and phase images were captured every 3 h for 48 h total. Fluorescent (infected) cells were quantified using the Incucyte software (https://downloads.essenbioscience.com/get/incucyte-2022b-rev2-gui).

RNA-sequencing

Cells were seeded 200,000 cells per well in a 12-well plate and incubated overnight. Next day cells were washed and media changed to VPSFM supplemented with 0.5 μg/ml TPCK-trypsin. After 4 h RNA was isolated (Direct-zol). mRNA sequencing was performed by Novogene using an Ilumina platform and polyA capture. Reads were aligned using HISAT2 and differential gene quantification done using DESeq2 (https://bioconductor.org/packages/release/bioc/html/DESeq2.html) (75, 76). Principal component analysis was performed using DESeq2. Gene set enrichment analysis was done using the molecular signatures database hallmark gene sets (77, 78). Genes for scatter plot of ISGs were based on molecular signatures database hallmark IFN response gene set. Matrix analysis was done using Morpheus software (https://software.broadinstitute.org/morpheus).

Western blot

Cells were seeded and incubated overnight in culture media. Cells were lysed in Laemmli buffer supplemented with beta-mercaptoethanol and HALT protease and phosphatase inhibitor cocktail (Sigma). Isolation of nuclei from whole-cell lysis adapted a standard centrifugation-based protocol (79). Briefly, cells were lysed in 0.1% Igepal in PBS supplemented with phosphatase inhibitor cocktail. Nuclear fractions were sedimented by centrifugation. Whole-cell lysates and nuclear fraction were resolved using SDS-PAGE. Western blot was done using a standard protocol, and images were processed and quantified using ImageJ (https://imagej.net/ij/download.html). For phospho-NF-kB experiments cells were serum starved for 4 to 8 h before lysing. Recombinant human TNF-α (R&D systems 210-TA) treatment was done at 20 ng/ml for 15 min before lysing cells. Recombinant human IFN-β (R&D systems 8499-IF-010) was done at 1000 IU/ml for 24 h before lysing cells. Antibodies used include: rabbit anti-JADE3 (Abcam #129495) used at 1:750 to 1:1000, rabbit anti-IFITM3 (Cell Signaling #59212) used at 1:750 to 1:1000, rabbit anti-NF-kB p65 (Cell Signaling #8242) used at 1:1000, rabbit anti-phospho-NF-kB p65 Ser536 (Cell Signaling #3033) used at 1:1000, rabbit anti-H3 (Cell Signaling), anti-Flag horseradish peroxidase (HRP) (Sigma), anti-rabbit IGG HRP (Sigma), and anti-GAPDH HRP (Sigma).

Quantitative-PCR

For qPCR of ΔJADE3 and JADE3 complementation experiments, cells were seeded 100,000 cells per well in a 24-well plate and incubated overnight. Next day, cells were washed and media changed to VPSFM supplemented with 0.25 μg/ml TPCK-trypsin. Recombinant human TNF-α treatment was done at 20 ng/ml for 6 h. Recombinant human IFN-β was done at 1000 IU/ml for 6 h. IAV PR8 infection was done at a MOI of 3 for 8 h. After treatment or infection, RNA was isolated using TRIzol and a Direct-zol kit (Zymo Research). cDNA prepared using a high-capacity cDNA reverse transcription kit (Thermo Fisher Scientific) and qPCR was performed using primers and probes from IDT (Fig. S7). Expression was normalized relative to the mRNA expression of actin.

Phylogenetic and sequence analysis

Ortholog gene groups for each of the JADE proteins were identified using NCBI orthologs (https://www.ncbi.nlm.nih.gov/kis/info/how-are-orthologs-calculated/). For Lamprey reciprocal blast hits were performed to find potential orthologs. Amino acid sequences were retrieved from NCBI (accession numbers in Fig. S9) and used for multiple sequence alignments using MAFFT (https://mafft.cbrc.jp/alignment/software/) (80, 81). Maximum likelihood trees were inferred by PhyML using 100 bootstrap replicates (82, 83). *Drosophila Melanogaster* Rhinoceros protein was used as an outgroup to root tree. Protein sequence alignment of human JADE proteins was done using NCBI's COBALT (84).

Data availability

Raw mapped read counts and STARS analysis from the CRISPRa screen are available in the Supplemental Tables. Normalized read counts and differentially expressed genes for all RNA sequencing from this study are also in the Supplemental Tables. All raw RNA sequencing data is deposited in the NCBI sequence read archive under the BioProject ID: PRJNA1022046.

Supporting information—This article contains supporting information.

Acknowledgments—We would like to thank Dr Peter Palese (Icahn School of Medicine at Mount Sinai) for the generous contributions of IAV strains and resources. We also would like to thank Dustin Hancks, John Schoggins, Julie Pfeiffer, and all members of the Orchard Lab for helpful discussions. Finally, we would like to thank Mikayla Olson for technical support.

Author contributions—M. M. and R. C. O. conceptualization; M. M., A. E., and J. G. D. investigation; M. M. and R. C. O. writing-original draft; M. M., A. E., J. G. D., N. S. H., C. B. W., and R. C. O. writing-review and editing; N. S. H. and C. B. W. resources; M. M., A. E., J. G. D., N. S. H., and C. B. W. methodology; M. M. visualization; R. C. O. funding acquisition.

Funding and additional information—M. M. was supported by the UT Southwestern Molecular Microbiology Training Grant (T32 AI007520). R. C. O. was supported by NIH grant R35GM142684. The content is solely the responsibility of the authors and does not necessarily represent the official views of the National Institutes of Health.

Conflict of interest—The authors declare that they have no conflict of interests with the contents of this article.

Abbreviations—The abbreviations used are: cDNA, complementary DNA; CRISPRa, CRISPR activation; FDR, false discovery rate; HBO1, histone acetyltransferase binding to ORC1; HRP, horseradish peroxidase; IAV, influenza A virus; IFITM3, interferon-induced transmembrane protein 3; ISG, interferon-stimulated gene; JADE3, Jade family PHD zinc finger 3; MOI, multiplicity of

infection; PHD, plant homeodomain; PR8, Puerto Rico/8/1934; qPCR, quantitative PCR; sgRNA, single guide RNA; TNF, tumor necrosis factor; TPCK-trypsin, L-1-tosylamido-2-phenylethyl chloromethyl ketone; VPSFM, virus production serum-free media.

References

1. Medzhitov, R. (2008) Origin and physiological roles of inflammation. *Nature* **454**, 428–435
2. Shalem, O., Sanjana, N. E., Hartenian, E., Shi, X., Scott, D. A., Mikkelson, T., *et al.* (2014) Genome-scale CRISPR-Cas9 knockout screening in human cells. *Science* **343**, 84–87
3. Wang, T., Wei, J. J., Sabatini, D. M., and Lander, E. S. (2014) Genetic screens in human cells using the CRISPR-Cas9 system. *Science* **343**, 80–84
4. Zablocki-Thomas, L., Menzies, S. A., Lehner, P. J., Manel, N., and Benaroch, P. (2020) A genome-wide CRISPR screen identifies regulation factors of the TLR3 signalling pathway. *Innate Immun.* **26**, 459–472
5. Schmid-Burgk, J. L., Chauhan, D., Schmidt, T., Ebert, T. S., Reinhardt, J., Endl, E., *et al.* (2016) A genome-wide CRISPR (clustered regularly interspaced short palindromic repeats) screen identifies NEK7 as an essential component of NLRP3 inflammasome activation. *J. Biol. Chem.* **291**, 103–109
6. Parnas, O., Jovanovic, M., Eisenhaure, T. M., Herbst, R. H., Dixit, A., Ye, C. J., *et al.* (2015) A genome-wide CRISPR screen in primary immune cells to dissect regulatory networks. *Cell* **162**, 675–686
7. Covarrubias, S., Vollmers, A. C., Capili, A., Boettcher, M., Shulkin, A., Correa, M. R., *et al.* (2020) High-throughput CRISPR screening identifies genes involved in macrophage viability and inflammatory pathways. *Cell Rep.* **33**, 108541
8. Schmidt, R., Steinhart, Z., Layeghi, M., Freimer, J. W., Bueno, R., Nguyen, V. Q., *et al.* (2022) CRISPR activation and interference screens decode stimulation responses in primary human T cells. *Science* **375**, eabj4008
9. Knott, G. J., and Doudna, J. A. (2018) CRISPR-Cas guides the future of genetic engineering. *Science* **361**, 866–869
10. Iwasaki, A., and Pillai, P. S. (2014) Innate immunity to influenza virus infection. *Nat. Rev. Immunol.* **14**, 315–328
11. Orchard, R. C., Sullender, M. E., Dunlap, B. F., Balce, D. R., Doench, J. G., and Virgin, H. W. (2019) Identification of antinorovirus genes in human cells using genome-wide CRISPR activation screening. *J. Virol.* **93**, e01324-18
12. Sanson, K. R., Hanna, R. E., Hegde, M., Donovan, K. F., Strand, C., Sullender, M. E., *et al.* (2018) Optimized libraries for CRISPR-Cas9 genetic screens with multiple modalities. *Nat. Commun.* **9**, 5416
13. Doench, J. G., Fusi, N., Sullender, M., Hegde, M., Vaimberg, E. W., Donovan, K. F., *et al.* (2016) Optimized sgRNA design to maximize activity and minimize off-target effects of CRISPR-Cas9. *Nat. Biotechnol.* **34**, 184–191
14. Brass, A. L., Huang, I. C., Benita, Y., John, S. P., Krishnan, M. N., Feeley, E. M., *et al.* (2009) The IFITM proteins mediate cellular resistance to influenza A H1N1 virus, West Nile virus, and dengue virus. *Cell* **139**, 1243–1254
15. Haller, O., Staeheli, P., Schwemmle, M., and Kochs, G. (2015) Mx GTPases: dynamin-like antiviral machines of innate immunity. *Trends Microbiol.* **23**, 154–163
16. Hubel, P., Urban, C., Bergant, V., Schneider, W. M., Knauer, B., Stukalov, A., *et al.* (2019) A protein-interaction network of interferon-stimulated genes extends the innate immune system landscape. *Nat. Immunol.* **20**, 493–502
17. Trimarco, J. D., Nelson, S. L., Chaparian, R. R., Wells, A. I., Murray, N. B., Azadi, P., *et al.* (2022) Cellular glycan modification by B3GAT1 broadly restricts influenza virus infection. *Nat. Commun.* **13**, 6456
18. de Vries, T., Knegtel, R. M., Holmes, E. H., and Macher, B. A. (2001) Fucosyltransferases: structure/function studies. *Glycobiology* **11**, 119R–128R
19. Oriol, R., Mollicone, R., Cailleau, A., Balanzino, L., and Breton, C. (1999) Divergent evolution of fucosyltransferase genes from vertebrates, invertebrates, and bacteria. *Glycobiology* **9**, 323–334
20. Merkulova, M., Păunescu, T. G., Azroyan, A., Marshansky, V., Breton, S., and Brown, D. (2015) Mapping the H+ (V)-ATPase interactome: identification of proteins involved in trafficking, folding, assembly and phosphorylation. *Sci. Rep.* **5**, 14827
21. Song, J., Chow, R. D., Peña-Hernández, M. A., Zhang, L., Loeb, S. A., So, E. Y., *et al.* (2022) LRRC15 inhibits SARS-CoV-2 cellular entry in trans. *PLoS Biol.* **20**, e3001805
22. Shilts, J., Crozier, T. W. M., Teixeira-Silva, A., Gabaev, I., Gerber, P. P., Greenwood, E. J. D., *et al.* (2023) LRRC15 mediates an accessory interaction with the SARS-CoV-2 spike protein. *PLoS Biol.* **21**, e3001959
23. Loo, L., Waller, M. A., Moreno, C. L., Cole, A. J., Stella, A. O., Pop, O. T., *et al.* (2023) Fibroblast-expressed LRRC15 is a receptor for SARS-CoV-2 spike and controls antiviral and antifibrotic transcriptional programs. *PLoS Biol.* **21**, e3001967
24. Heaton, B. E., Kennedy, E. M., Dumm, R. E., Harding, A. T., Sacco, M. T., Sachs, D., *et al.* (2017) A CRISPR activation screen identifies a pan-avian influenza virus inhibitory host factor. *Cell Rep.* **20**, 1503–1512
25. Harding, A. T., Heaton, B. E., Dumm, R. E., and Heaton, N. S. (2017) Rationally designed influenza virus vaccines that are antigenically stable during growth in eggs. *mBio* **8**, e00669-17
26. Rebendenne, A., Roy, P., Bonaventure, B., Chaves Valadão, A. L., Desmarets, L., Arnaud-Arnould, M., *et al.* (2022) Bidirectional genome-wide CRISPR screens reveal host factors regulating SARS-CoV-2, MERS-CoV and seasonal HCoVs. *Nat. Genet.* **54**, 1090–1102
27. Foy, R. L., Song, I. Y., Chitalia, V. C., Cohen, H. T., Saksouk, N., Cayrou, C., *et al.* (2008) Role of Jade-1 in the histone acetyltransferase (HAT) HBO1 complex. *J. Biol. Chem.* **283**, 28817–28826
28. Tzouanacou, E., Tweedie, S., and Wilson, V. (2003) Identification of Jade1, a gene encoding a PHD zinc finger protein, in a gene trap mutagenesis screen for genes involved in anteroposterior axis development. *Mol. Cell. Biol.* **23**, 8553–8562
29. Lalonde, M. E., Avvakumov, N., Glass, K. C., Joncas, F. H., Saksouk, N., Holliday, M., *et al.* (2013) Exchange of associated factors directs a switch in HBO1 acetyltransferase histone tail specificity. *Genes Dev.* **27**, 2009–2024
30. Shahbazian, M. D., and Grunstein, M. (2007) Functions of site-specific histone acetylation and deacetylation. *Annu. Rev. Biochem.* **76**, 75–100
31. Pancer, Z., Amemiya, C. T., Ehrhardt, G. R. A., Ceitlin, J., Gartland, G. L., and Cooper, M. D. (2004) Somatic diversification of variable lymphocyte receptors in the agnathan sea lamprey. *Nature* **430**, 174–180
32. Ujie, M., Takada, K., Kiso, M., Sakai-Tagawa, Y., Ito, M., Nakamura, K., *et al.* (2019) Long-term culture of human lung adenocarcinoma A549 cells enhances the replication of human influenza A viruses. *J. Gen. Virol.* **100**, 1345–1349
33. Sanchez, R., and Zhou, M. M. (2011) The PHD finger: a versatile epigenome reader. *Trends Biochem. Sci.* **36**, 364–372
34. Doyon, Y., Cayrou, C., Ullah, M., Landry, A. J., Côté, V., Selleck, W., *et al.* (2006) ING tumor suppressor proteins are critical regulators of chromatin acetylation required for genome expression and perpetuation. *Mol. Cell* **21**, 51–64
35. Saksouk, N., Avvakumov, N., Champagne, K. S., Hung, T., Doyon, Y., Cayrou, C., *et al.* (2009) HBO1 HAT complexes target chromatin throughout gene coding regions *via* multiple PHD finger interactions with histone H3 tail. *Mol. Cell* **33**, 257–265
36. Schoggins, J. W. (2019) Interferon-stimulated genes: what do they all do? *Annu. Rev. Virol.* **6**, 567–584
37. Bailey, C. C., Huang, I. C., Kam, C., and Farzan, M. (2012) Ifitm3 limits the severity of acute influenza in mice. *PLoS Pathog.* **8**, e1002909
38. Everitt, A. R., Clare, S., Pertel, T., John, S. P., Wash, R. S., Smith, S. E., *et al.* (2012) IFITM3 restricts the morbidity and mortality associated with influenza. *Nature* **484**, 519–523
39. Wu, X., Dao Thi, V. L., Huang, Y., Billerbeck, E., Saha, D., Hoffmann, H. H., *et al.* (2018) Intrinsic immunity shapes viral resistance of stem cells. *Cell* **172**, 423–438.e25
40. Wakim, L. M., Gupta, N., Mintern, J. D., and Villadangos, J. A. (2013) Enhanced survival of lung tissue-resident memory CD8+ T cells during infection with influenza virus due to selective expression of IFITM3. *Nat. Immunol.* **14**, 238–245

41. Sakurai, H., Chiba, H., Miyoshi, H., Sugita, T., and Toriumi, W. (1999) IkappaB kinases phosphorylate NF-kappaB p65 subunit on serine 536 in the transactivation domain. *J. Biol. Chem.* **274**, 30353–30356
42. Huang, B., Yang, X. D., Lamb, A., and Chen, L. F. (2010) Posttranslational modifications of NF-kappaB: another layer of regulation for NF-kappaB signaling pathway. *Cell. Signal.* **22**, 1282–1290
43. Biering, S. B., Sarnik, S. A., Wang, E., Zengel, J. R., Leist, S. R., Schäfer, A., *et al.* (2022) Genome-wide bidirectional CRISPR screens identify mucins as host factors modulating SARS-CoV-2 infection. *Nat. Genet.* **54**, 1078–1089
44. Dukhovny, A., Lamkiewicz, K., Chen, Q., Fricke, M., Jabrane-Ferrat, N., Marz, M., *et al.* (2019) A CRISPR activation screen identifies genes that protect against Zika virus infection. *J. Virol.* **93**, e00211-19
45. Danziger, O., Patel, R. S., DeGrace, E. J., Rosen, M. R., and Rosenberg, B. R. (2022) Inducible CRISPR activation screen for interferon-stimulated genes identifies OAS1 as a SARS-CoV-2 restriction factor. *PLoS Pathog.* **18**, e1010464
46. King, C. R., Liu, Y., Amato, K. A., Schaack, G. A., Mickelson, C., Sanders, A. E., *et al.* (2023) Pathogen-driven CRISPR screens identify TREX1 as a regulator of DNA self-sensing during influenza virus infection. *Cell Host Microbe* **31**, 1552–1567.e8
47. Zhu, X., Trimarco, J. D., Williams, C. A., Barrera, A., Reddy, T. E., and Heaton, N. S. (2022) ZBTB7A promotes virus-host homeostasis during human coronavirus 229E infection. *Cell Rep.* **41**, 111540
48. Kueh, A. J., Dixon, M. P., Voss, A. K., and Thomas, T. (2011) HBO1 is required for H3K14 acetylation and normal transcriptional activity during embryonic development. *Mol. Cell. Biol.* **31**, 845–860
49. Mishima, Y., Miyagi, S., Saraya, A., Negishi, M., Endoh, M., Endo, T. A., *et al.* (2011) The Hbo1-Brd1/Brpf2 complex is responsible for global acetylation of H3K14 and required for fetal liver erythropoiesis. *Blood* **118**, 2443–2453
50. MacPherson, L., Anokye, J., Yeung, M. M., Lam, E. Y. N., Chan, Y. C., Weng, C. F., *et al.* (2020) HBO1 is required for the maintenance of leukaemia stem cells. *Nature* **577**, 266–270
51. Kenney, A. D., Zani, A., Kawahara, J., Eddy, A. C., Wang, X. L., Mahesh, K. C., *et al.* (2023) Interferon-induced transmembrane protein 3 (IFITM3) limits lethality of SARS-CoV-2 in mice. *EMBO Rep.* **24**, e56660
52. Gómez-Herranz, M., Taylor, J., and Sloan, R. D. (2023) IFITM proteins: understanding their diverse roles in viral infection, cancer, and immunity. *J. Biol. Chem.* **299**, 102741
53. Das, T., Yang, X., Lee, H., Garst, E. H., Valencia, E., Chandran, K., *et al.* (2022) S-palmitoylation and sterol interactions mediate antiviral specificity of IFITMs. *ACS Chem. Biol.* **17**, 2109–2120
54. Amini-Bavil-Olyaee, S., Choi, Y. J., Lee, J. H., Shi, M., Huang, I. C., Farzan, M., *et al.* (2013) The antiviral effector IFITM3 disrupts intracellular cholesterol homeostasis to block viral entry. *Cell Host Microbe* **13**, 452–464
55. Chesarino, N. M., Compton, A. A., McMichael, T. M., Kenney, A. D., Zhang, L., Soewarna, V., *et al.* (2017) IFITM3 requires an amphipathic helix for antiviral activity. *EMBO Rep.* **18**, 1740–1751
56. Zhang, Q., Lenardo, M. J., and Baltimore, D. (2017) 30 Years of NF-κB: a blossoming of relevance to human pathobiology. *Cell* **168**, 37–57
57. Liu, T., Zhang, L., Joo, D., and Sun, S. C. (2017) NF-κB signaling in inflammation. *Signal. Transduct. Target. Ther.* **2**, 17023
58. Uhlen, M., Karlsson, M. J., Zhong, W., Tebani, A., Pou, C., Mikes, J., *et al.* (2019) A genome-wide transcriptomic analysis of protein-coding genes in human blood cells. *Science* **366**, eaax9198
59. Schmiedel, B. J., Singh, D., Madrigal, A., Valdovino-Gonzalez, A. G., White, B. M., Zapardiel-Gonzalo, J., *et al.* (2018) Impact of genetic polymorphisms on human immune cell gene expression. *Cell* **175**, 1701–1715.e16
60. Rahman, M. M., and McFadden, G. (2011) Modulation of NF-κB signalling by microbial pathogens. *Nat. Rev. Microbiol.* **9**, 291–306
61. Albarnaz, J. D., Ren, H., Torres, A. A., Shmeleva, E. V., Melo, C. A., Bannister, A. J., *et al.* (2022) Molecular mimicry of NF-κB by vaccinia virus protein enables selective inhibition of antiviral responses. *Nat. Microbiol.* **7**, 154–168
62. Flory, E., Weber, C. K., Chen, P., Hoffmeyer, A., Jassoy, C., and Rapp, U. R. (1998) Plasma membrane-targeted Raf kinase activates NF-kappaB and human immunodeficiency virus type 1 replication in T lymphocytes. *J. Virol.* **72**, 2788–2794
63. Yoshida, H., Kato, N., Shiratori, Y., Otsuka, M., Maeda, S., Kato, J., *et al.* (2001) Hepatitis C virus core protein activates nuclear factor kappa B-dependent signaling through tumor necrosis factor receptor-associated factor. *J. Biol. Chem.* **276**, 16399–16405
64. Wang, X., Li, M., Zheng, H., Muster, T., Palese, P., Beg, A. A., *et al.* (2000) Influenza A virus NS1 protein prevents activation of NF-kappaB and induction of alpha/beta interferon. *J. Virol.* **74**, 11566–11573
65. Pauli, E.-K., Schmolke, M., Wolff, T., Viemann, D., Roth, J., Bode, J. G., *et al.* (2008) Influenza A virus inhibits type I IFN signaling *via* NF-κB-dependent induction of SOCS-3 expression. *PLoS Pathog.* **4**, e1000196
66. Wang, S., Chi, X., Wei, H., Chen, Y., Chen, Z., Huang, S., *et al.* (2014) Influenza A virus-induced degradation of eukaryotic translation Initiation factor 4B contributes to viral replication by suppressing IFITM3 protein expression. *J. Virol.* **88**, 8375–8385
67. Latreille, E., and Lee, W. L. (2023) Modulation of the host response as a therapeutic strategy in severe lung infections. *Viruses* **15**, 1462
68. Dam, S., Kracht, M., Pleschka, S., and Schmitz, M. L. (2016) The influenza A virus genotype determines the antiviral function of NF-κB. *J. Virol.* **90**, 7980–7990
69. Wurzer, W. J., Ehrhardt, C., Pleschka, S., Berberich-Siebelt, F., Wolff, T., Walczak, H., *et al.* (2004) NF-kappaB-dependent induction of tumor necrosis factor-related apoptosis-inducing ligand (TRAIL) and Fas/FasL is crucial for efficient influenza virus propagation. *J. Biol. Chem.* **279**, 30931–30937
70. Santoro, M. G., Rossi, A., and Amici, C. (2003) NF-κB and virus infection: who controls whom. *EMBO J.* **22**, 2552–2560
71. Clement, M., Forbester, J. L., Marsden, M., Sabberwal, P., Sommerville, M. S., Wellington, D., *et al.* (2022) IFITM3 restricts virus-induced inflammatory cytokine production by limiting Nogo-B mediated TLR responses. *Nat. Commun.* **13**, 5294
72. Jiang, L. Q., Xia, T., Hu, Y. H., Sun, M. S., Yan, S., Lei, C. Q., *et al.* (2018) IFITM3 inhibits virus-triggered induction of type I interferon by mediating autophagosome-dependent degradation of IRF3. *Cell. Mol. Immunol.* **15**, 858–867
73. Sanjana, N. E., Shalem, O., and Zhang, F. (2014) Improved vectors and genome-wide libraries for CRISPR screening. *Nat. Methods* **11**, 783–784
74. Reed, L. J., and Muench, H. (1938) A simple method of estimating fifty per cent endpoints. *Am. J. Epidemiol.* **27**, 493–497
75. Kim, D., Paggi, J. M., Park, C., Bennett, C., and Salzberg, S. L. (2019) Graph-based genome alignment and genotyping with HISAT2 and HISAT-genotype. *Nat. Biotechnol.* **37**, 907–915
76. Love, M. I., Huber, W., and Anders, S. (2014) Moderated estimation of fold change and dispersion for RNA-seq data with DESeq2. *Genome Biol.* **15**, 550
77. Subramanian, A., Tamayo, P., Mootha, V. K., Mukherjee, S., Ebert, B. L., Gillette, M. A., *et al.* (2005) Gene set enrichment analysis: a knowledge-based approach for interpreting genome-wide expression profiles. *Proc. Natl. Acad. Sci. U. S. A.* **102**, 15545–15550
78. Liberzon, A., Birger, C., Thorvaldsdóttir, H., Ghandi, M., Mesirov, J. P., and Tamayo, P. (2015) The Molecular Signatures Database (MSigDB) hallmark gene set collection. *Cell Syst.* **1**, 417–425
79. Suzuki, K., Bose, P., Leong-Quong, R. Y., Fujita, D. J., and Riabowol, K. (2010) REAP: a two minute cell fractionation method. *BMC Res. Notes* **3**, 294
80. Katoh, K., and Standley, D. M. (2013) MAFFT multiple sequence alignment software version 7: improvements in performance and usability. *Mol. Biol. Evol.* **30**, 772–780
81. Zimmermann, L., Stephens, A., Nam, S. Z., Rau, D., Kübler, J., Lozajic, M., *et al.* (2018) A completely reimplemented MPI bioinformatics toolkit with a new HHpred server at its core. *J. Mol. Biol.* **430**, 2237–2243
82. Guindon, S., Dufayard, J. F., Lefort, V., Anisimova, M., Hordijk, W., and Gascuel, O. (2010) New algorithms and methods to estimate maximum-likelihood phylogenies: assessing the performance of PhyML 3.0. *Syst. Biol.* **59**, 307–321
83. Lefort, V., Longueville, J. E., and Gascuel, O. (2017) SMS: smart model selection in PhyML. *Mol. Biol. Evol.* **34**, 2422–2424
84. Papadopoulos, J. S., and Agarwala, R. (2007) COBALT: constraint-based alignment tool for multiple protein sequences. *Bioinformatics* **23**, 1073–1079